Post-treatment with Ferrostatin-1 alleviates acute kidney injury in mice by inhibiting ferroptosis

3 Yanxiu Zhao[1], Binhua Jiang[2], Dinghui Huang[3], Juxiang Lou[1], Guoshun Li[1], Jianqi Liu[1], Fuhui
4 Duan[1], Yuan Yuan[4*], Xiaoyan Su[1*]

5 [1] Department of Nephrology, Baoshan People's Hospital, Qingbao Road, Longyang District,
6 Baoshan City, Yunnan Province, 678000, China

7 [2] Department of Obstetrics, Baoshan People's Hospital, Qingbao Road, Longyang District,
8 Baoshan City, Yunnan Province, 678000, China

9 [3] Department of Pediatrics, Baoshan People's Hospital, Qingbao Road, Longyang District,
10 Baoshan City, Yunnan Province, 678000, China

11 [4] Intensive Care Unit, Ningbo Medical Center Lihuili Hospital, Ningbo University, No. 1111
12 Jiangnan Road, Ningbo, 315040, Zhejiang Province, China.

13 *Correspondence to:

14 Yuan Yuan, Intensive Care Unit, Ningbo Medical Center Lihuili Hospital, Ningbo University,
15 No. 1111 Jiangnan Road, Ningbo, 315040, Zhejiang Province, China

16 , Email address: yuanyuan1040@163.com

17 Xiaoyan Su, Department of Nephrology, Baoshan People's Hospital, Qingbao Road, Longyang
18 District, Baoshan City, Yunnan Province, 678000, China, Email address:
19 Su13987058543@163.com

20 **Running Title: Ferrostatin-1 AKI Mitigation via Ferroptosis Inhibition in Mice**

Abstract

22 **Background**: Acute kidney injury (AKI) is a common and serious medical condition with high
23 morbidity and mortality.Recent research has highlighted ferroptosis, a novel form of
24 programmed cell death, as a potential therapeutic target in mitigating renal tubular injury in AKI.
25 Ferrostatin-1, a specific ferroptosis inhibitor, has been demonstrated to prevent renal injury
26 through ferroptosis inhibition.

27 **Methods** :Utilizing a murine AKI model, we investigated the effects of Ferrostatin-1 by
28 administering it post-injury. Through high-throughput sequencing and pathological analysis, we
29 focused on the critical role of ferroptosis-related pathways in the treatment.

30 **Results**: Ferrostatin-1 post-conditioning effectively mitigated oxidative damage and reduced iron
31 content associated with AKI. Additionally, critical ferroptosis-related proteins, such as GPX4,

32   SLC7A11, NRF2, and FTH1, exhibited increased expression levels. In vitro, Ferrostatin-1
33   treatment of HK-2 cells significantly diminished lipid peroxidation and iron accumulation.
34   Furthermore, Ferrostatin-1 was found to downregulate the PI3K signalling pathway.

35   **Conclusion**:Ferrostatin-1 acted as a potential ferroptosis inhibitor with the capacity to enhance
36   antioxidant defences. This study suggests that Ferrostatin-1 could serve as a promising novel
37   strategy for improving the treatment of AKI and promoting recovery from the condition.

38   **Keywords**: Iron death, Acute kidney injury, Ferrostatin-1

39

1. Introduction

Acute kidney injury (AKI), typified by a rapid deterioration in renal function, is a common and serious medical condition with high morbidity and mortality. Often secondary to extrarenal events, AKI affects approximately 30% of critically ill patients and 5% of hospitalized patients [1]. The molecular mechanisms underlying AKI remain incomplete, and current prevention and treatment options are limited. Finding effective drugs that can preserve renal function and improve the prognosis of AKI in clinical practice is an urgent need.

Ferroptosis, a recently identified cell death mode, is different from necrosis, and is characterized by a unique morphological phenotype, excessive accumulation of lipid peroxides, and increased levels of free iron [2]. This cell death pathway has been implicated in diseases, such as Parkinson's and Alzheimer's, cancer, stroke, ischemia-reperfusion injury, intracranial haemorrhage, and brain injury. Numerous studies have recently established a potential association between ferroptosis and AKI [3-8].

Glutathione peroxidase 4 (GPX4), a key biomarker of ferroptosis, is responsible for reducing lipid peroxide, which requires glutathione (GSH) as the substrate[9]. System Xc− is an amino acid reverse transport protein that exists in the cell membrane and is composed of SLC7A11 and SLC3A2 heterodimers. The transport system Xc− is responsible for the exchange of intracellular glutamate and extracellular cystine[10]. Cystine could be converted into Cysteine in the cell and becomes the synthesis substrate of GSH. GSH further cooperates with GPX4 to exert an antioxidant effect and maintain cellular redox balance. Therefore, the inactivation or abnormal expression of system Xc− will affect the ability of cells to process ROS. Studies have found that if the total amount of amino acids (especially cystine) in serum were deficient in vitro, it would cause rapid cell death. Later, it was confirmed that this type of cell death is ferroptosis [11]. Early studies have confirmed that system Xc− is abundant in the brush border membrane of renal tubular cells (anatomically, the part where the kidney mainly carries out amino acid transport) [12]. Inhibition of system Xc− or ischemic state will lead to the lack of amino acid supply, intracellular GSH level decreased, and the antioxidant capacity diminished, leading to ferroptosis and renal tubular injury. In addition, ferritin heavy chain 1 (FTH1) is responsible for intracellular iron storage. NF-E2-related factor 2 (NRF2) is the transcription regulator of GPX4, SLC7A11, FTH1 and other iron death-related proteins. These factors were considered biomarkers of ferroptosis.

Recent studies have shown that ferroptosis plays a crucial role in regulating AKI. Ferroptosis was observed in various types of AKI, such as AKI induced by cisplatin, rhabdomyolysis, ischemia/reperfusion, or folic acid. The purpose of this study was to confirm that Ferrostatin-1, a candidate ferroptosis inhibitor, may reduce AKI by reversing ferroptosis and alleviating lipid peroxidation and iron accumulation in vitro model and in vivo model. We then explored the pathway involved by transcriptome analysis, expecting to provide a new strategy for the clinical treatment of AKI.

2 Materials & Methods

2.1 Cell culture and treatment

Human proximal tubular epithelial cells (HK-2 cells) were cultured in a atmosphere comprised of 95% air and 5% CO_2 at 37 ℃. HK-2 cells were seeded into culture plates at 5×10^5 cells/well and cultured 24 h before each experiment. Subsequently, we added LPS (10 μg/ml) into the cultured cells for 22 h to establish the cell model of LPS-induced AKI[13]. Then, Ferrostatin-1 was added into the HK-2 cells according to previous study [14]. The HK-2 cells were divided into 3 groups: the control group, LPS-induced (10 μg/ml) AKI group, and LPS-induced (10 μg/ml) + Ferrostatin-1 (1 μM) group. The experiments were approved by the Ethics Committee of Baoshan people's Hospital(SYSU-IACUC-2020-A0327).

2.2 Animals and experimental protocol

C57BL/6 mice weighing 20-25 g were procured for this study and housed in a temperature and humidity-controlled environment with a 12-hour light-dark cycle, while being fed standard food and water ad libitum. The study was approved by the Animal Ethics Committee of Baoshan People's Hospital. The AKI model in vivo was established as previously described [15]. All mice received intraperitoneal administration of pentobarbital (50 mg/kg) and AKI was induced via cecal ligation and puncture (CLP) with a 22-gauge needle. The sham/Con group mice underwent the same procedure without cecal ligation or puncture. Subsequently, pre-warmed normal saline at a dosage of 1 ml per 25 g body weight was administered subcutaneously. At 5 h after CLP, either normal saline (NS, 0.5 ml, vehicle) or Ferrostatin-1 (ferrostatin-1, 1.5 mg/kg, a ferroptosis inhibitor; Sigma-Aldrich, MO, United States) was intravenously administered. At 24 h after intravenous injection, the animals were euthanized and blood and kidney tissues were collected for further experiments. The mice were divided into three groups: the Sham/Con group, the CLP group, and the CLP + Ferrostatin-1 (1 μM) group.

Animal care, including feeding, housing, and enrichment, was carried out according to established guidelines. Criteria for euthanizing animals were established prior to the planned end of the experiment. Any surviving animals at the conclusion of the experiment were monitored and accounted for accordingly.

2.3 BUN and Cr Detection

The serum gathered from the blood samples by centrifugation (3000 rpm, 5 min, 4 ℃) were used to evaluate renal function. The levels of serum BUN and Cr were detected by the commercial assay kit - Urea assay kit (Nanjing Jiancheng, China) and Creatinine assay kit (sarcosine oxidase)(Nanjing Jiancheng, China), according to the manufacturer's instructions, respectively.

111 **2.4 ROS Detection**

112 The level of ROS in the renal tissues was determined by Dihydroethidium (DHE) fluorescence
113 with a DCFH-DA assay kit. Renal tissues were stored at -20 °C until the fluorescence assay. The
114 blocks were cut on polylysine-coated glass slides and incubated with 10 μM DHE for 30 min at
115 37 °C and then incubated with DAPI solution at room temperature for 10 min, kept in the dark
116 place. Wshing the tissues with PBS 3 times at room temperature, and the tissues were then
117 incubated with the DCFH-DA staining solution for 1 h at 37℃. Images were captured using a
118 fluorescence microscope.

119

120 The levels of ROS in HK-2 cells were also tested by the DCFH-DA assay kit following the
121 manufacturer's instructions. HK-2 cells were seeded on 35 mm laser confocal petri dishes at a
122 density of $1:0 \times 10^5$ cells per well and cultured at 37℃ for 24 h with 95% air and 5% CO_2. The
123 HK-2 cells were treated with Ferrostatin-1 (1 μM) for 24 h and then were treated with DCFH-
124 DA for 20 min in dark. After that, the HK-2 cells were washed with PBS 3 times to remove
125 DCFH-DA and the images of samples were captured by a fluorescence microscope.

126 **2.5 Histopathological Analysis**

127 The renal samples were dissected and fixed with paraformaldehyde. Then, renal samples were
128 paraffin-embedded, sliced into 4-μm slices, and stained with HE (hematoxylin and eosin) [16].
129 The specimens were evaluated in a blinded manner.

130 **2.6 Quantitative real-time polymerase chain reaction**

131 RNA was extracted and real-time polymerase chain reaction (PCR) of HK-2 cells and kidney
132 samples were performed [17]. The PCR reaction volume was 20 μl, including 30 ng RNA as the
133 template and 12 μl SYBR Green PCR Master Mix (Applied Biosystems). Gpx4 forward primer
134 sequences were 5′-CCGGCTACAATGTCAGGTTT-3′ and reverse primer sequences were 5′-
135 ACGCAGCCGTTCTTATCAAT-3′; SLC7A11 forward primer sequences were 5′-
136 GATGCTGTGCTTGGTCTTGA-3′ and reverse primer sequences were 5′-GCCTAC
137 CATGAGCAGCTTTC-3′; NRF2 forward primer sequences were 5′-
138 CTTTTATCTCACTTTACCGCCCGAG-3′ and reverse primer sequences were 5′-
139 GACACGTGGGAGTTCAGAGGG-3′ and FTH1 forward primer sequences were 5′-
140 ATGATGTGGCCCTGAAGAAC-3′ and reverse primer sequences were 5′-
141 TCATCACGGTCAGGTTTCTG-3′. PCR conditions were 95 ℃ for 5 min, followed by 36
142 cycles of 30 s at 94.5 °C, 30 s at 60 °C, and 60 s at 72 °C, and at 72 °C for 7 min as the final
143 extension. The relative expression of the genes of each specimen was analyzed using a
144 comparative CT method with $2^{-\triangle\triangle Ct}$.

145 **2.7 Western Blot Analysis**

146 We performed Western blot as previously recorded [18,19]. Firstly, the proteins extracted from
147 renal tissues or HK-2 cells were lysed with RIPA solution, proteins were collected and their
148 concentrations were determined, followed by electrophoresis in 10% SDS-polyacrylamide gel.
149 After electrophoresis, the proteins were transferred to PVDF membrane, sealed with TBST
150 blocking solution containing 5% nonfat milk powder for 2 h. The primary antibody was added
151 and incubated at 4 °C overnight, followed by the second antibody incubated at room temperature
152 for 2 h. After washing the blots, chemiluminescent reagent was added. The band images were
153 taken by ImageJ gel software and the gray value of the detected protein was calculated.

154 **2.8 Detection of Glutathione (GSH) and Malondialdehyde (MDA) Levels**

155 The levels of malondialdehyde (MDA) and glutathione (GSH) in HK-2 cells and kidney tissues
156 were determined with the commerical assay kit purchased from Nanjing Jiancheng
157 Bioengineering Institute (Nanjing, China), following the respective manufacturer's instructions.
158 A microplate fluorometer read individual levels of MDA and GSH at 532 or 405 nm according to
159 the manufacturer's instructions, respectively[20].

160 **2.9 Iron assay**

161 Intracellular and tissue levels of total iron were assessed using an iron assay kit (Sigma-Aldrich).

162 Total iron levels in HK-2 cells or kidney tissue samples were measured using an iron assay kit
163 (Sigma-Aldrich). HK-2 cells or kidney tissue samples were harvested and homogenized in iron
164 assay buffer and centrifuged. 10 μl supernatant was mixed with 90 μl iron analysis buffer and 5μl
165 iron reductant. The mixture was incubated for 30 min and the total iron levels were measured
166 using an iron probe with a wavelength of 593nm.

167 **2.10 Transcriptome sequencing**

168 Samples were collected from the Ferrostatin-1 and AKI groups (n = 3 of each group). The
169 samples were put into the enzyme-free Eppendorf tubes. After the samples were frozen in liquid
170 nitrogen, they were wrapped in dry ice and transported to the company for total RNA extraction
171 and sequencing processing. Use high-throughput sequencing to analyze differentially expressed
172 genes and find relevant pathways.

173 **2.11 Statistical analysis**

174 All data in this study was expressed as mean ± standard deviation (SD) and was analyzed using
175 SPSS statistical software package (SPSS, Inc., Chicago, IL, USA). Differences between means
176 were compared using the Student's t-test. One-way analysis of variance (ANOVA) and Dunnett

177 multiple comparison test were also used for analysis, and a P value $<$ 0.05 was considered
178 statistically significant.

3. Results

3.1 Ferrostatin-1 treatment Protects Against AKI in the mice Model

181 The impact of Ferrostatin-1 on the AKI was confirmed by adding Ferrostatin-1 to the AKI group.
182 Figure 1A shows significant pathological changes in the AKI model. In the Sham/Control group,
183 the renal tissue morphology was normal, the structure was clear, the cells were regularly
184 arranged, and there was no inflammation or fiber exudation; while in the AKI model group, there
185 was brush like edge damage, proximal tubular dilation, interstitial widening, proteinaceous casts
186 and necrosis. Compared with the AKI model group, the Ferrostatin-1-treatment group showed
187 alleviated pathological changes of brush like edge damage, proximal tubular dilation, interstitial
188 widening, proteinaceous casts and necrosis. As shown in Figure 1C and Figure 1D, compared
189 with the Sham/Control group, the concentration of serum BUN and Cr in the AKI model group
190 was significantly higher. And the levels of serum BUN and Cr were decreased after the
191 administration of Ferrostatin-1, but still higher than those of the Sham/Control group. These
192 results indicated that Ferrostatin-1 can significantly mitigate kidney injury.

3.2 Ferrostatin-1 Attenuates Ferroptosis During AKI

194 To further prove that the protection of Ferrostatin-1 on AKI referred to Ferroptosis, the tissue
195 ROS production and lipid ROS level (MDA and GSH) were measured. AKI markedly increased
196 the generation of ROS and MDA levels and decreased the GSH activity, whereas Ferrostatin-1
197 post-conditioning inhibited the oxidative damage caused by AKI (Figure 1B, Figure 1E, F).
198 Secondly, the iron content and the expressions of GPX4, SLC7A11, NRF2 and FTH1 were
199 valued. In the AKI model group, the iron content (Figure 1G) increased while the expressions of
200 GPX4, SLC7A11, NRF2 and FTH1 decreased. However, post-treatment with Ferrostatin-1
201 suppressed these alterations (Figure 2). These finding suggested that post-treatment with
202 Ferrostatin-1 mitigated AKI by inhibiting ferroptosis.

3.3 Ferrostatin-1 Mitigates Ferroptosis in LPS-Induced HK2 Cells

204 Based on the findings mentioned earlier *in vivo*, we next evaluated the function of Ferrostatin-1
205 on LPS-induced AKI. In Figure 3A, there were significant pathological changes in the LPS-
206 induced AKI model, such as brush border damage, proximal tubule dilation, interstitial widening,
207 proteinaceous casts and necrosis. As shown in Figure 3B, post-treatment with Ferrostatin-1
208 induced ROS levels in LPS-induced AKI group. Similarly, post-treatment with Ferrostatin-1
209 prevented the decrease of the GPX4, SLC7A11, NRF2 and FTH1 expression in the Ferrostatin-1
210 treatment group (Figure 3C-K). Obviously, Ferrostatin-1 inhibited LPS-induced ferroptosis *in*
211 *vitro*.

212 **3.4 Ferrostatin-1 Inhibits LPS-Induced Ferroptosis Through the PI3K Pathway *In Vitro***

213 To fully understand the molecular mechanisms involved in the AKI, we performed high-
214 throughput transcriptional sequencing to identify differentially expressed genes (DEGs) between
215 the Ferrostatin-1 and LPS groups (n = 3 in each group). A total of 63677 genes were identified in
216 the RNA-seq data set. The heatmap showed 5099 DEGs in the Ferrostatin-1 and LPS groups
217 (Figure 4A). Furthermore, the volcano plot (Figure 4B) revealed 35 upregulated, and 26
218 downregulated DEGs in the Ferrostatin-1 group. The DEGs were also used for GO/KEGG
219 analysis; the phosphatidylinositol 3−kinase signalling (PI3K) pathway was involved (Figure 4C),
220 suggesting that ferroptosis may be associated with AKI. Consequently, these results further
221 supported that Ferrostatin-1 may induce AKI in mice through ferroptosis by the PI3K pathway.

222 # 4. Discussion

223 The kidney, a vulnerable organ, significantly impacts septic patients' outcomes, as renal injury
224 contributes to prolonged hospital stays and increased mortality rates [21,22]. Plenty of studies
225 have established a correlation between the lipid peroxidation and ROS in AKI. Ferroptosis, a
226 novel iron-dependent, lipid peroxidation-induced cell death pathway, has been recently identified
227 [15]. The recent study investiged the effect of ferrostatin-1 and its potential efficacy in AKI
228 therapy. The pivotal findings of this study encompass ferroptosis' involvement in AKI, the
229 protective effect of Ferrostatin-1 post-treatment against AKI via ferroptosis inhibition, and
230 Ferrostatin-1's protective mechanism's reliance on the PI3K pathway [21-23].

231

232 Recent investigations have revealed that the inhibition of GPX4 could diminish reduction of lipid
233 peroxides[24]. GPX4 utilizes GSH and eliminates lipid peroxides [25]. Several studies have
234 demonstrated that Ferrostatin-1 can inhibit ferroptosis and alleviate acute kidney injury[26,27].
235 In line with these findings, our study also revealed that post-treatment with Ferrostatin-1 could
236 mitigate AKI. Since ferroptosis occurs during AKI, Ferrostatin-1 may offer a promising strategy
237 for AKI prevention.

238 However, our study presents the following limitations. Firstly, our focus was on the impact of
239 ferrostatin-1 on ferroptosis. Although the direct anti-ferroptosis effects of ferrostatin-1 were
240 proved, we did not examine its influence on other types of cell death, such as autophagy and
241 necroptosis. Secondly, the precise mechanism through which ferrostatin-1 modulates the PI3K
242 pathway warrants further investigation.

5. Conclusions

In summary, AKI triggers ferroptosis by increasing iron contents and lipid peroxidation. Ferrostatin-1, acting as a ferroptosis inhibitor, enhances antioxidant capacity and effectively alleviates AKI by inducing the gene expression of lipid metabolism enzymes within the PI3K pathway. This study offers compelling evidence supporting the potential application of ferrostatin-1 in the treatment of AKI.

Data Availability Statement

This statement indicates that the article and any supplementary material contain the original contributions of the study. Readers who have further inquiries regarding the study can contact the corresponding authors for more information.

Ethics Statement

The ethical considerations of this study involving human participants were reed and approved by the Animal Ethics Committee of Baoshan People's Hospital. All patients/participants provided written informed consent to participate in the study, and all procedures were conducted in accordance with the ethical standards outlined in the Declaration of Helsinki.

Author Contributions

Yanxiu Zhao performed the experiments, prepared figures and/or tables, authored or reviewed drafts of the paper, and approved the final draft.

Binhua Jiang, Dinghui Huang, and Juxiang Lou analyzed the data, prepared figures and/or tables, and approved the final draft.

Guoshun Li, Jianqi Liu, Fuhui Duan, and Yuan Yuan conceived and designed the experiments, analyzed the data, prepared figures and/or tables, authored or reviewed drafts of the paper, and approved the final draft.

Yuan Yuan and Xiaoyan Su conceived and designed the experiments, analyzed the data, authored or reviewed drafts of the paper, and approved the final draft.

Conflict of Interest

The authors declare that they have no competing interests.

6. References

[1] Bellomo R , Kellum J A , Ronco C . Acute kidney injury.[J]. Lancet, 2012, 380(9843):756-766.

[2] Dixon S , Lemberg K , Lamprecht M , et al. Ferroptosis: an iron-dependent form of nonapoptotic cell death.[J]. Cell, 2012, 149(5).

[3] Linkermann A , Brasen J H , Darding M , et al. Two independent pathways of regulated necrosis mediate ischemia–reperfusion injury[J]. Proceedings of the National Academy of Sciences of the United States of America, 2013, 110(29):12024-12029.

[4] Scindia Y , Dey P , Thirunagari A , et al. Hepcidin Mitigates Renal Ischemia-Reperfusion Injury by Modulating Systemic Iron Homeostasis.[J]. Journal of the American Society of Nephrology Jasn, 2015, 26(11):2800.

[5] Tonnus W , Linkermann A . The in vivo evidence for regulated necrosis[J]. Immunological Reviews, 2017, 277.

[6] Friedmann Angeli J P , Schneider M , Proneth B , et al. Inactivation of the ferroptosis regulator Gpx4 triggers acute renal failure in mice[J]. Free Radical Biology & Medicine, 2014, 76(12):1180-1191.

[7] Linkermann, Andreas, Skouta, et al.. Synchronized renal tubular cell death involves ferroptosis.

[8] Yang W , Sriramaratnam R , Welsch M , et al. Regulation of Ferroptotic Cancer Cell Death by GPX4[J]. Cell, 2014, 156(1-2):317-331.

[9] Ursini F , Maiorino M . Lipid peroxidation and ferroptosis: The role of GSH and GPx4[J]. Free Radical Biology and Medicine, 2020, 152.

[10] Bridges R J , Natale N R , Patel S A . System xc cystine/glutamate antiporter: an update on molecular pharmacology and roles within the CNS.[J]. British Journal of Pharmacology, 2012(1):165.

[11] Gao M , Monian P , Quadri N , et al. Glutaminolysis and Transferrin Regulate Ferroptosis[J]. Molecular Cell, 2015, 59(2):298-308.

[12] Burdo, J. Distribution of the cystine/glutamate antiporter system xc- in the brain, kidney, and duodenum.[J]. Journal of Histochemistry & Cytochemistry, 2006, 54(5):549-557.

[13] Sun M , Li J , Mao L , et al. p53 Deacetylation Alleviates Sepsis-Induced Acute Kidney Injury by Promoting Autophagy[J]. Frontiers in Immunology, 2021, 12:685523.

[14] Qiang Zhuanzhuan,Dong Hui,Xia Yangyang et al. Nrf2 and STAT3 Alleviates Ferroptosis-

304   Mediated IIR-ALI by Regulating SLC7A11.[J] .Oxid Med Cell Longev, 2020, 2020: 5146982.

305   [15]Miyaji T , Hu X , Yuen P S T , et al. Ethyl pyruvate decreases sepsis-induced acute renal
306   failure and multiple organ damage in aged mice[J]. Kidney international, 2003, 64(5):1620-31.

307   [16]Adipose-Derived Mesenchymal Stem Cell Protects Kidneys against Ischemia-Reperfusion
308   Injury through Suppressing Oxidative Stress and Inflammatory Reaction.[J]. Journal of
309   Translational Medicine, 2010.

310   [17 Kang S , Adler S , Lapage J , et al. p38 MAPK and MAPK kinase 3/6 mRNA and
311   activities are increased in early diabetic glomeruli.[J]. Kidney international, 2001, 60(2):543-52.

312   [18]Zhang J , Zhang Y , Xiao F , et al. The peroxisome proliferator-activated receptor
313   gamma agonist pioglitazone prevents NF-kappa B activation in cisplatin nephrotoxicity through
314   the reduction of p65 acetylation via the AMPK-SIRT1/p300 pathway[J]. Biochemical
315   Pharmacology, 2016(101-):101.

316   [19]Fei L , Jingyuan X , Fangte L , et al. Preconditioning with rHMGB1 ameliorates lung
317   ischemia-reperfusion injury by inhibiting alveolar macrophage pyroptosis via the
318   Keap1/Nrf2/HO-1 signaling pathway.[J]. Journal of translational medicine, 2020, 18(1):301.

319   [20]Gao Y , Zeng Z , Li T , et al. Polydatin Inhibits Mitochondrial Dysfunction in the Renal
320   Tubular Epithelial Cells of a Rat Model of Sepsis-Induced Acute Kidney Injury[J]. Anesthesia
321   and Analgesia, 2015, 121(5):1251-1260.

322   [21]Peerapornratana S , Manrique-Caballero C L , H Gómez, et al. Acute kidney injury from
323   sepsis: current concepts, epidemiology, pathophysiology, prevention and treatment[J]. Kidney
324   International, 2019, 96(5):1083-1099.

325   [22]Poston J T , Koyner J L . Sepsis associated acute kidney injury[J]. BMJ, 2019.

326   [23]Fani Filippo,Regolisti Giuseppe,Delsante Marco et al. Recent advances in the pathogenetic
327   mechanisms of sepsis-associated acute kidney injury.[J] .J Nephrol, 2018, 31: 351-359.

328   [24]Pengxu, Lei, Tao, et al.. Mechanisms of Ferroptosis and Relations With Regulated Cell
329   Death: A Review.[J]. Frontiers in Physiology, 2019.

330   [25]Hadian K , Stockwell B R . SnapShot: Ferroptosis[J]. Cell, 2020, 181(5):1188-1188.e1.

331   [26]Scindia Y , Leeds M J , Swaminathan M S . Iron Homeostasis in Healthy Kidney and its
332   Role in Acute Kidney Injury[J]. Seminars in Nephrology, 2019, 39(1):76-84.

333   [27]Swelm R P L V , Wetzels J F M , Swinkels D W . The multifaceted role of iron in renal
334   health and disease[J]. Nature Reviews Nephrology.

Figure 1

Ferrostatin-1 attenuates CLP-induced kidney injury.

Mice were given a sham operation or CLP model operation, with or without ferrostatin-1 (Ferrostatin-1) administration. (A) Representative images (200 ×) showing HE staining of renal sections (scale bar = 50 μm) (B) Representative images of TEM (scale bar = 50 μm). (C) The quantification of the DHE fluorescence intensity of ROS. (D) BUN concentration in the plasma. (E) Creatinine (Cr) concentration in the plasma. The levels of MDA (F), GSH (G), and Fe2+ (H) in mouse kidney homogenates(n = 5). *p < 0.05 vs. Sham group, p < 0.05 vs. CLP group, P <0.05 vs. Fe group, and p > 0.05 vs CLP group. Data are presented as mean ± SD (n = 10).
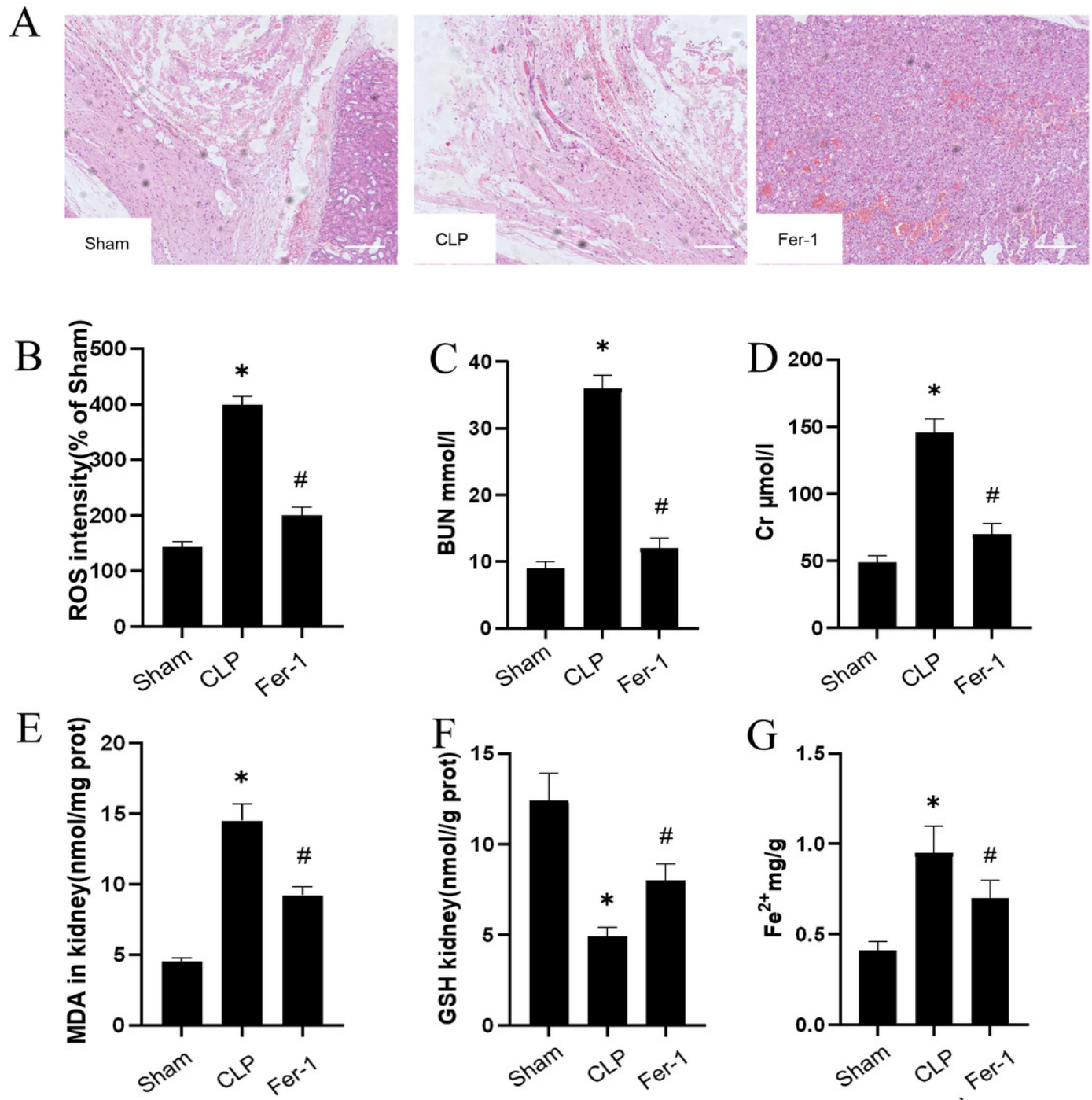
Figure 2

Ferrostatin-1 alleviates the occurrence of ferroptosis in AKI.

(A-D) Quantitation of GPX4 , SLC7A11, NRF2 and FTH1 gene expression. (E) Western blot analysis of GPX4, SLC7A11, NRF2 and FTH1 proteins in the kidney tissue. (n = 3). *p < 0.05 vs. Sham group, #p < 0.05 vs. CLP group, &p < 0.05 vs. Fe group. Data are presented as mean ± SD.
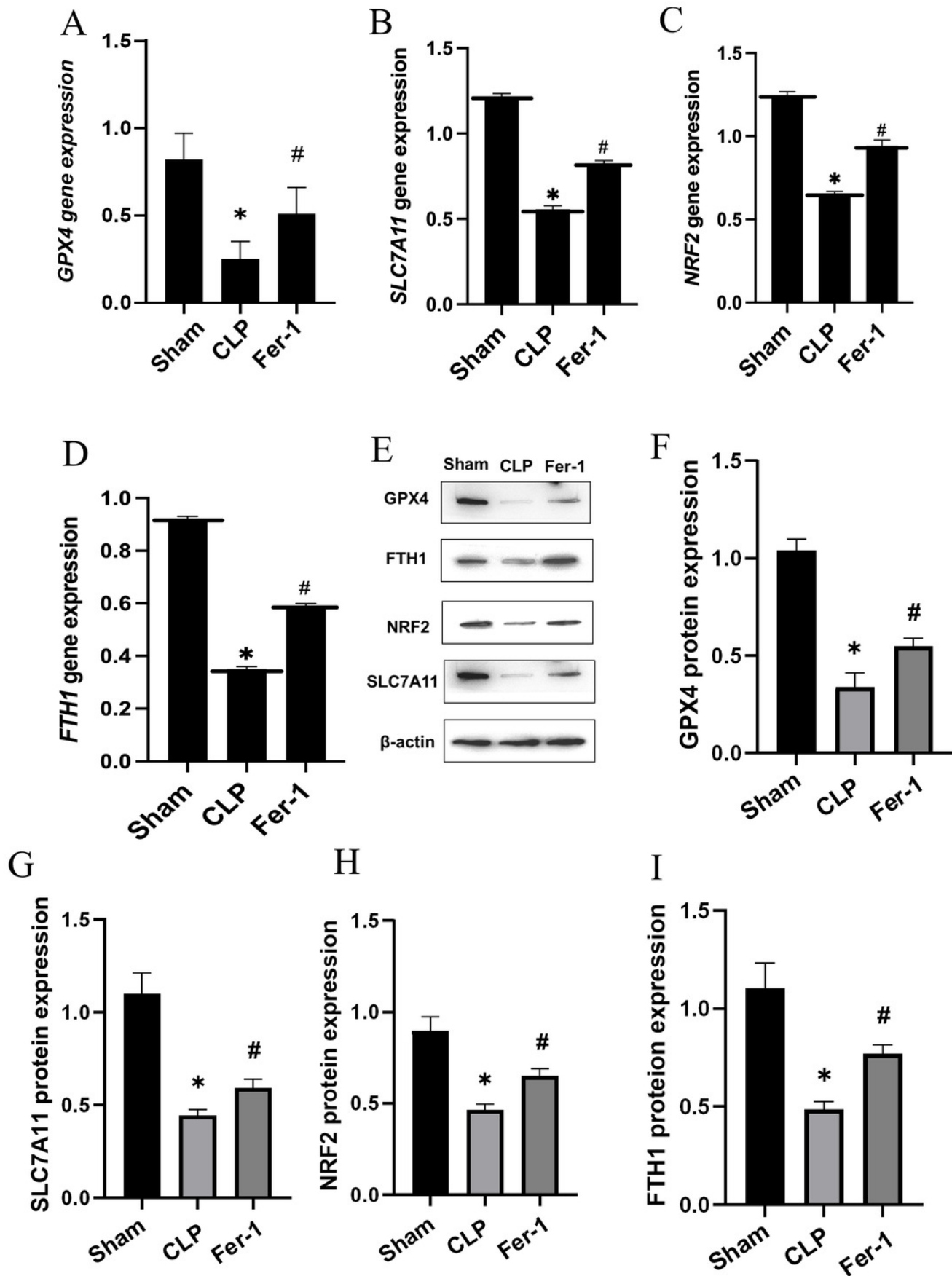
Figure 3

Ferrostatin-1 inhibits LPS-induced ferroptosis in HK-2 cells.

(A) Representative images (200 ×) showing HE staining of renal sections (scale bar = 50 µm) (B) Representative images of TEM (scale bar = 50 µm). (C) The quantification of the DCFH-DA fluorescence intensity of ROS. (D-G) Quantitation of GPX4 , SLC7A11, NRF2 and FTH1 gene expression. (H) Western blot analysis of GPX4, SLC7A11, NRF2 and FTH1 proteins in the HK-2 cells. (n = 3). *p < 0.05 vs. Sham group, #p < 0.05 vs. CLP group, &p < 0.05 vs. Fe group. Data are presented as mean ± SD.
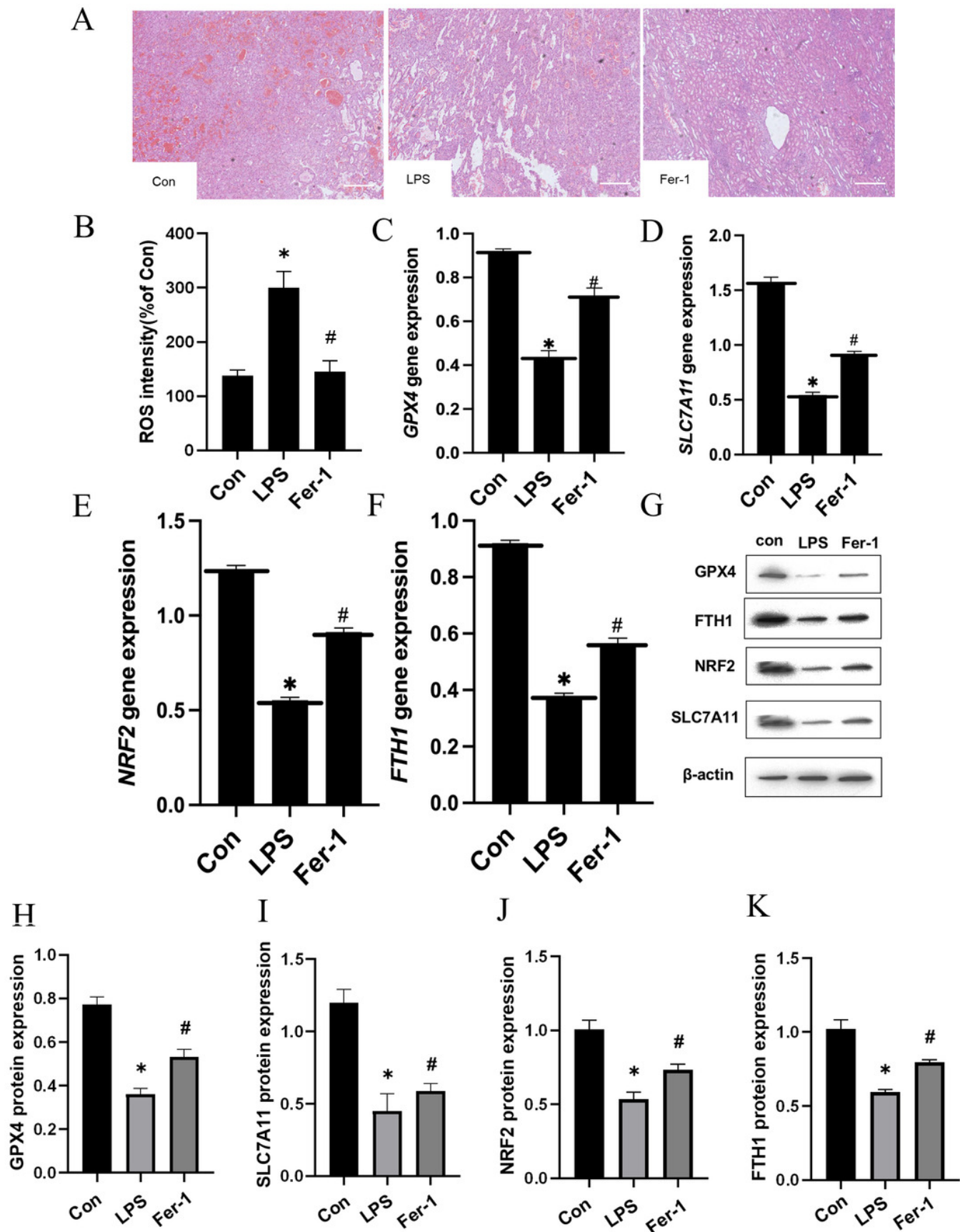
Figure 4

HK-2 cells were involved in transcriptome sequencing.

(A) Heatmap showed the hierarchical cluster analysis of the differentially expressed genes (DEGs) in HK-2 cells. (B) volcano plot represented the overall distribution of gene expression levels and differential multiples between the LPS group and Ferrostatin-1 group. (C) Enrichment analysis of the Gene Ontology (GO) signalling pathway in the Ferrostatin-1 group compared with the LPS group assayed by RNA-sequencing of HK-2 cells.